Alpha-particle production in the ^{6}He+^{120}Sn collision.

R. Lichtenthäler^a, S. Appannababu^h, M. A. G. Alvarez^b, M. Rodríguez-Gallardo^b, A. Lépine-Szily^a, K.C.C. Pires^a, O.C.B. Santos^a, U. Umbelino^a, P.N. de Faria^c, V. Guimarães^a, E.O.N. Zevallos^a, V. Scarduelli^a, M. Assunção^d, J.M.B. Shorto^e, A. Barioni^f, J. Alcántara-Núñez^a, V. Morcelle^g and A. Serra^a.

^{a}Instituto de Física, Universidade de São Paulo, 05508-090, São Paulo, Brazil.
^{b}Departamento de FAMN, Universidad de Sevilla, Apto. 1065, E-41080 Sevilla, Spain.
^{c}Departamento de Física, Universidade Federal Fluminense do Rio de Janeiro, 24210-310, Rio de Janeiro, Brazil.
^{d}Departamento de Física, Universidade Federal de São Paulo -UNIFESP-, CEP 09913-030, Diadema Brazil.
^{e}Instituto de Pesquisas Energéticas e Nucleares - IPEN, 05508-000, São Paulo, Brazil.
^{f} Departamento de Ciências do Mar, Universidade Federal de São Paulo, UNIFESP, São Paulo, Brazil.
^{g}Departamento de Física, Universidade Federal Rural do Rio de Janeiro, 23851-970, Rio de Janeiro, Brazil.
^{h}Department of Nuclear Physics, Andhra University, Visakhapatnam, India - 530 003.
Instituto de Física da Universidade de São Paulo, 05508-090, São Paulo, BR

E-mail: rubens@if.usp.br

Abstract. Alpha particle energy distributions in the ^{6}He+^{120}Sn collision have been measured at 7 bombarding energies above the Coulomb barrier. A phenomenological analysis of the centroids of the experimental distributions was performed and compared with the expected alpha-particle energies from breakup and neutron transfer reactions. Q-optimum conditions were determined using the Brinks formula for the di-neutron transfer reaction. A comparison of the measured alpha-particle production cross-sections with Continuum Discretized Coupled Channels (CDCC) calculations for breakup is presented.

1. Introduction

Light nuclei usually have small breakup energies compared to heavier nuclei. Stable light nuclei such as ^{6,7}Li, ^{9}Be and others have breakup energies in the range 1.5-2.5 MeV which are small compared to breakup energies around 7 MeV usually found in heavier stable nuclei such as Carbon and Oxygen. As we move away from the stability valley we find even more weakly bound nuclei such as ^{6}He, ^{11}Li, ^{11}Be with breakup energies below 1 MeV or even lower values such as 0.13 MeV for the proton rich ^{8}B. In addition, some of these so called exotic nuclei present a 'halo' structure formed by the loosely bound nucleons around a more bound core. Owing to their low binding energies and low angular momentum, the wave function of the valence nucleons usually extends to large distances from the central core. As a consequence, exotic nuclei usually have a larger total reaction cross-section compared to similar stable projectiles, even at low bombarding energies [1–7]. The reaction channels which are contributing to the enhancement in

the reaction cross section is still an open question. Projectile breakup, incomplete fusion, total fusion and neutron transfers [8] are candidates.

In this contribution we present data on the ^{120}Sn(^{6}He,α)X reaction at energies above the Coulomb barrier [9]. The alpha-particles emitted from this reaction were detected at fixed laboratory angles for 7 different ^{6}He beam energies and their energy distribution was analysed.

2. Experiment

The experiment was performed at the Pelletron accelerator of the University of São Paulo using the RIBRAS (Radioactive Ion Beams in Brasil) system to produce the ^{6}He secondary beam. A ^{7}Li primary beam of about 300 nAe impinged on a 16 μm ^{9}Be primary target. The ^{6}He particles produced by the ^{9}Be(^{7}Li, ^{6}He) transfer reaction were collected and focused by the first solenoid. The acceptance cone of the first solenoid comprises angles between $2 \deg \leq \theta \leq 6 \deg$ (see Figure 1) [10–12].
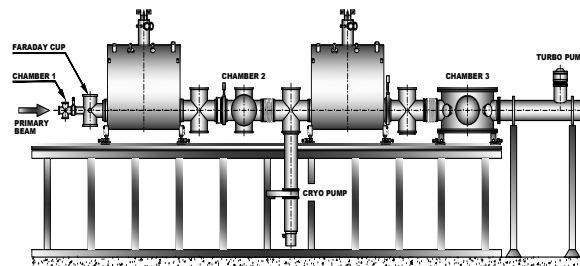

Figure 1. RIBRAS scheme.

The secondary beam can be focused either in chamber 2, where a secondary target and detectors can be mounted, or in chamber 3 after the second solenoid. In chamber 2 the beam is usually contaminated with particles from the degraded primary beam as well as other light particles such as alphas, protons, deuterons and tritons which have the same magnetic rigidity. To improve the beam purity a degrader foil can be placed in the central chamber allowing a further selection by the second solenoid. This procedure usually improves the beam purity to more than 95% compared to 16% in chamber 2 in the case of ^{6}He beam.

The detection system consists of silicon detector telescopes E(1000μm)-ΔE(25μm) capable of identifying the mass, charge and energy of the particles emerging from the target. Two secondary targets were used in the experiments, a 3.8 mg/cm^2 ^{120}Sn target and a 4mg/cm^2 Gold target to normalize the cross-sections.

Two experiments have been performed, one in chamber 2 where an excitation function at 60 deg was measured and another in chamber 3 at 22.2 MeV. In the latter a 2 mg/cm^2 Gold foil was used as degrader in chamber 2 to provide a differential energy loss and subsequent selection by the second solenoid.

In Figure 2 we show an E-ΔE spectrum obtained in scattering chamber 3.

The spectra have been calibrated using an ^{241}Am alpha source and the ^{6}He elastic scattering peak energy as determined from the solenoid current [13]. The residual energy E and ΔE signals have been summed to obtain the total energy axis as in Figure 2.
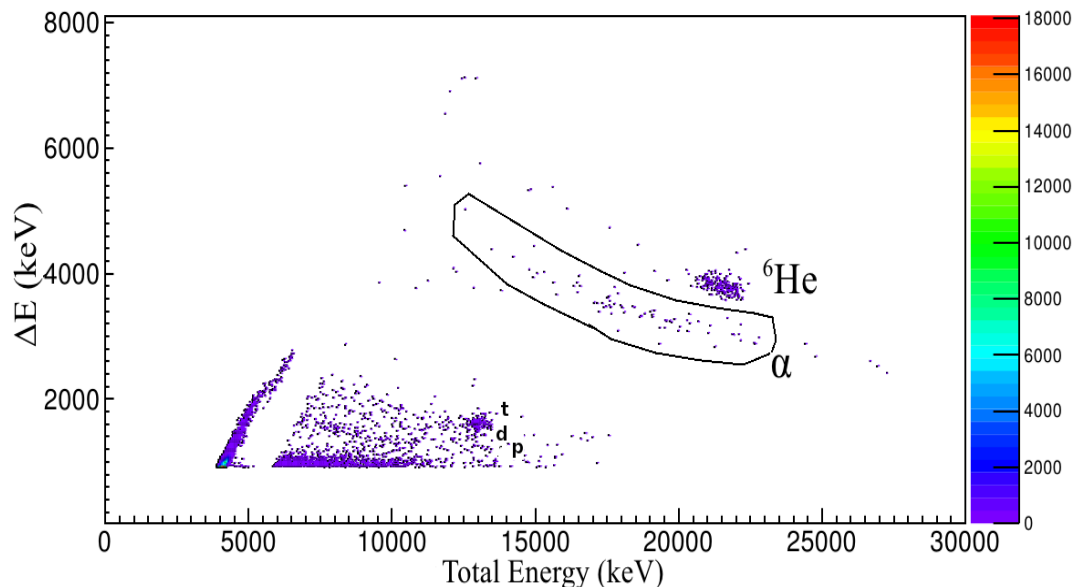

Figure 2. ΔE-E$_{total}$ spectrum for the reaction ^{6}He + ^{120}Sn at 22.2 MeV and 36^0 [9] using the two solenoids of RIBRAS.

One sees the elastic scattering peak well separated from the alpha-particles produced in the ^{120}Sn(^{6}He,α)X reaction.

3. Results

The resulting alpha-particle energy distributions obtained at 60 deg at different bombarding energies is shown in Figure 3 (left). In Figure 3 (right) we show the same distributions transforming the energy of the alpha-particles (x-axis) to Q-value of the di-neutron transfer reaction ^{120}Sn(^{6}He,α)^{122}Sn. There is a unique relation between $E_\alpha \to Q$, given the two-body kinematics of the transfer reaction. The Q-centroids of the distributions are shown by the black arrows.

The alpha-particle energy distribution at 22.2 MeV and differential cross-sections at three angles are shown in Figure 5 left and right respectively. An excitation function of the energy integrated alpha-particle production at 60 deg is shown in Figure 6.

4. Discussion

We see from Figure 3 that the centroids of the energy distributions are located at energies considerably larger than the values predicted by projectile breakup ($E_{bu} \approx \frac{2}{3}E_{6He}$) where E_{6He} is the bombarding energy. The Q-value centroids are located around Q=0 shifting to negative Q-values as the bombarding energies increase. Theoretically, Q=0 is expected as the optimum-Q in the case of zero angular momentum ($l_t = 0$) neutron transfer reactions. A more precise value of Q-optimum can be obtained from the well known Brink's formula [15] which depends on the angular momentum transferred in the collision. In figure 4 we plot the ^{122}Sn excitation energy as a function of the square of the transfer angular momentum as obtained from Brink's formula using the experimental centroids of the Q-optimum for each bombarding energy. The
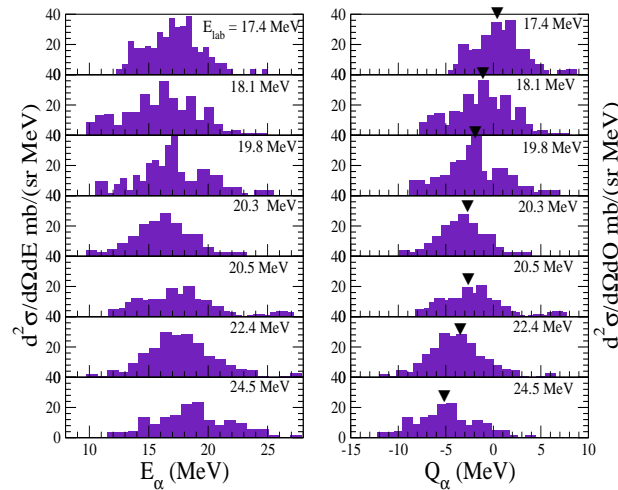
Figure 3. Alpha-particle energy distributions at 60 degrees for different ^{6}He bombarding energies (left). The same with the energy axis transformed to Q-value for the di-neutron transfer reaction $^{120}Sn(^6He,\alpha)^{122}Sn$ (right) [9].
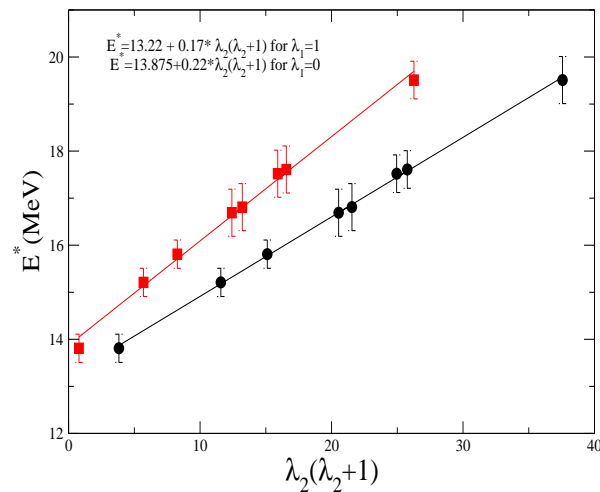

Figure 4. Excitation energy versus the square of the final angular momentum of the di-neutron in the ^{120}Sn(^{6}He,α)^{122}Sn transfer reaction for two different initial angular momenta $\lambda_1 = 0$ (red squares) and $\lambda_1 = 1$ (black dots) [9].

excitation energies have been obtained directly from the energy distributions $E_{exc} = Q_{gs} - Q_{av}$ where $Q_{gs} = 14.01$ MeV and Q_{av} are the centroids of the distributions from Figure 3.

We see in Figure 4 that, for di-neutron initial angular momentum ($\lambda_1 = 1$, black dots) a linear relation is obtained between excitation energy and the square of the final angular momentum.
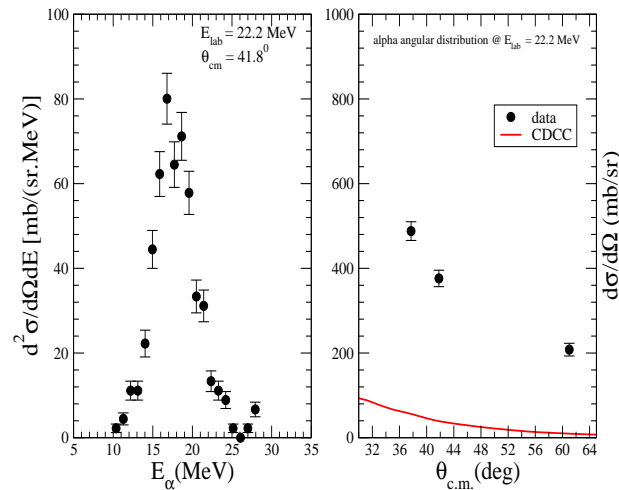
Figure 5. Projection of the alpha-particle energy distribution at E_{6He}=22.2 MeV (left), differential cross-sections at three angles (right) compared to 4b-CDCC calculations.
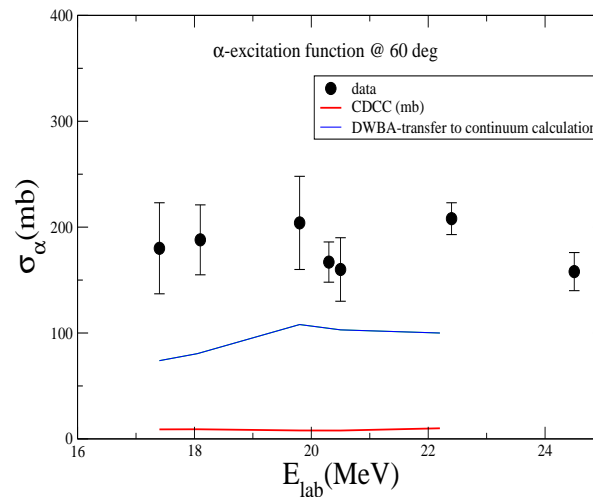

Figure 6. Alpha-particle cross-sections measured at 60 deg for different bombarding energies compared to 4b-CDCC and DWBA transfer to continuum (TC) calculations

The moment of inertia that comes out from this plot is close to what is expected for a 2n-^{120}Sn rotating system driven by the di-neutron momentum transfer in the collision.

It is clear from Figures 5 and 6 that the measured alpha-production cross sections are much larger than the 4b-CDCC breakup predictions [14] indicating that a process other than pure projectile breakup is taking place.

5. Conclusions.

Cross sections for alpha-particle production in the ^{6}He + ^{120}Sn collision at energies above the Coulomb barrier have been measured. A kinematical analysis of the α-particle energy distributions in terms of the Q-value for the two-neutron stripping reaction $^{120}Sn(^6He,\alpha)^{122}Sn$ was performed. The results show that the α-particle energy distributions are centered at Q-values around zero (optimum Q-value for neutron transfer) going to negative values $Q \approx -5.5$ MeV, as the bombarding energy increases from 17.4 to 24.5 MeV. These Q-values show that the recoil system ^{120}Sn+$2n$ is formed in highly excited states in the continuum. Using Brink's formula for Q-optimum transfer, we interpret the decrease in the reaction Q-value as being due to a corresponding increase in the transferred angular momentum. We found that the final excitation energies follow a linear relation with the square of the final angular momentum, indicating that some kind of di-nuclear rotating system could be formed.

The measured α-particle production cross sections are very large indicating the presence of reaction mechanisms other than pure projectile breakup. In order to confirm the present results, further measurements would be required to obtain information on the recoil nuclei and its final angular momentum.

5.1. Acknowledgments

References

[1] de Faria P N *et al.* 2010 *Phys. Rev. C* **81** 044605
[2] de Faria P N *et al.* 2010 *Phys. Rev. C* **82** 034602
[3] Pires K C C *et al.* 2011 *Phys. Rev. C* **83** 064603
[4] Pires K C C *et al.* 2014 *Phys. Rev. C* **90** 027605
[5] Morcelle V *et al.*, 2017 *Phys. Rev. C* **95** 014615
[6] Morcelle V *et al.* 2014 *Physics Letters* B **732** 228
[7] Pires K C C, Appannababu S, Lichtenthäler R and Santos O C B 2018 *Phys. Rev.* C **98**, 014614
[8] Morcelle V *et al.* 2019 *Phys. Rev. C* **99** 064617
[9] Appannababu S, Lichtenthäler R, Alvarez M A G, Rodríguez-Gallardo M, Lépine-Szily A, Pires K C C, Santos O C B, Silva U U , de Faria P N, Guimaraes V, Zevallos E O N, Scarduelli V, Assunção M, Shorto J M B, Barioni A, Alcantara-Nunez J and Morcelle V 2019 *Phys. Rev. C* **99** 014601
[10] Lichtenthäler R *et al.* 2016 *Few-Body Systems* **57** 157
[11] Lépine-Szily A, Lichtenthäler R, Guimarães V, 2014 *Eur. Phys. J.* A **50**, 128
[12] Lichtenthäler R, Lépine-Szily A, Guimarães V *et al.* 2005 *Eur. Phys. J. A* **25**, 733
[13] Lichtenthäler R *TWSP RIBRAS beam transport code* unpublished
[14] Rodríguez-Gallardo M *et al.* 2008 *Phys. Rev. C* **77** 064609
[15] Brink D M 1972 *Physics Letters* **40B**, 37